Journal of Materials Chemistry B

Accepted Manuscript

ROYAL SOCIETY OF CHEMISTRY

www.rsc.org/materialsB

Journal Name

RSCPublishing

ARTICLE

Flexible Pressure Sensing Film Based on Ultra-sensitive SWCNT/PDMS Spheres for Monitoring Human Pulse Signals

Yan-Long Tai, Zhen-Guo Yang*

Cite this: DOI: 10.1039/x0xx00000x

Received 00th January 2012,
Accepted 00th January 2012

DOI: 10.1039/x0xx00000x

www.rsc.org/

Flexible pressure sensors are essential components of electronic skin for future attractive applications ranging from human healthcare monitoring to biomedical diagnostics to robotic skins to prosthetic limbs. Here, we report a new kind of flexible pressure sensing film based on ultrasensitive single wall carbon nanotube (SWCNT)/polydimethylsiloxane (PDMS) sphere. These spheres with the diameter 600 ± 20 um were prepared by dipping method, and were further sandwiched by flexible electrodes using a stack of double-sided tape. The sensing mechanism of this device was analyzed by classic thin plate theory for circulate plate deflection. Its sensitivity was further optimized by synthesis of sensitive materials and geometrical design of device parameters. Ultimately, the developed sensing film exhibited a maximum sensitivity of 46.7 % kPa^{-1} to resistance, great durability over 15,000 cycles, and very rapid mechanical responses (a few milliseconds). We also demonstrated that our sensing film can be used to detect the location and distribution of finger pressure, as well as to mapping the fingertip pulse signals, jugular venous pulse (JVP) signals and wrist pulse signals of the testers of different ages effectively.

1. Introduction

Flexible pressure sensors, as essential parts of electronic skin (E-skin) detecting human subtle pulse pressure changes (<10 kPa, approximating gentle touch), have drawn more attention in recent years. [1-5] Such E-skins have already present very attractive future applications like human healthcare monitoring, [6] biomedical diagnostics, [7] robotic skins, [8] and prosthetic limbs. [9] In human healthcare monitoring, pressure sensors should be capable of measuring the human pulse with sufficient spatial and temporal resolution. Then, the key information features can be returned accordingly in the form of frequency, rhythm, shape, and strength, etc… [10, 11] At present, it is difficult to establish the relationship directly between the pressurized pulse signals and specific health conditions. But, they are indeed closely related, in particularly relevant to cardiovascular disease (CVD) including all the diseases of the heart and circulation, such as coronary heart disease, angina, heart attack, congenital heart disease and stroke. [12, 13, 14]

Currently, although some integrated complementary metal–oxide–semiconductor (CMOS) devices exhibit high pressure sensitivity and stability, they show poor portable ability, high manufacturing cost and are not environmental friendly. [15,16] Thus, several technologies for flexible pressure sensors were reported, such as ultrathin Au nanowire based piezoresistive sensors [7], nanowire active array field-effect transistor [3], polydimethylsiloxane (PDMS) and carbon nanotube/graphene nanosheet based sensor [10, 17], microstructured rubber dielectric layer capacitors [18]. The proposed techniques face similar problems: fabrication of complicated micro/nano-structure, challenging scalability, high cost, and demanding materials. Therefore, the design and manufacture of portable, highly sensitive, reproducible and cost effective pressure biosensors are strongly desirable.

Polydimethylsiloxane (PDMS) a silicone elastomer with its inherent biocompability, excellent physical viscoelasticity, simple to manipulate, and low cost. These desirable properties make it very attractive for the development of E-skin devices, not only for substrate, but also for electrical sensing materials. These have been proved to give higher sensitivity, faster response time and great durability. As for substrate, a conductive coating should be deposited on the surface of PDMS film by curing/peeling-off process first. Thus, the sensitive mechanism is from piezoresistive effect of the deposited conductive coating along with the deformation of PDMS substrate. [19] However, repeatability and reliability is not easy to control. As for electrical sensing materials, typically, conductive filler was added into PDMS matrix, then structured PDMS film was fabricated by a silicon mold. The

geometry and shape of micro-features can be well-controlled by the mold. [17, 18] But, the fabrication of silicon mold is complicated and expensive, requiring multi-steps (spin coating, lithography, and etching, etc…), and large area integration with nanomaterial assemblies is also less reproducible. Presently, PDMS elastomer sphere has been prepared effectively by dipping method used for bio-device, [20, 21, 22] whereas PDMS based conductive sphere and its application for electronic skin have not been reported.

Here, we demonstrate a simple process for the development of a flexible pressure sensing film based on ultrasensitive SWCNT/PDMS sphere. First, SWCNT/PDMS composite elastomer was prepared. The concentration of SWCNT was chose closer to the percolation threshold to maximize the piezoresistive sensitivity of the elastomer. Then, the configuration of this sensing elastomer was used to prepare conductive sphere by the reproducible dipping method with superfine glass fiber (diameter = 125 μm). Second, these conductive spheres were further sandwiched between two polyethylene terephthalate (PET) films with patterned electrodes. A small preload on the sphere was created, and the resulted contact geometry can be easily disturbed under an external mechanical pressure. Accordingly, the sensing mechanism of this device was analyzed by thin plate theory for circulate plate deflection.

The constructed flexible pressure sensing film will be characterized by its mechanical-resistance response with different diameters of the sensing area and applied loading values. The excellent performance will be presented, such as high sensitivity, very rapid mechanical response, a large working pressure range, great durability and repeatability. In addition, this pressure sensing film will demonstrate the capability to detect the location and distribution of finger pressure, as well as to mapping the fingertip pulse signals, jugular venous pulse (JVP) signals and wrist pulse signals of the testers of different ages effectively. Moreover, the entire preparation and fabrication process of such pressure sensing film is fully compatible with the industrial-scale manufacturing of portable/wearable medical devices, which permits scalable production at a significantly lower unit-cost.

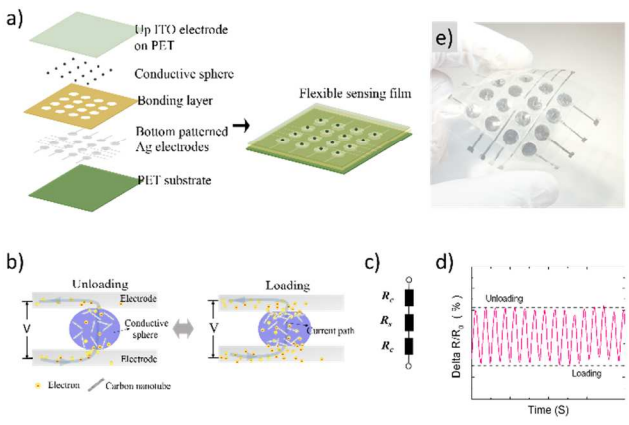

Fig.1 a) Schematic illustration of the assembling structure of the flexible sensing film, consisting of ITO electrode on PET as up skin, patterned Ag electrodes on PET as bottom skin, a stack of double-sided tape as bonding frame, and ultrasensitive SWCNT/PDMS sphere as sensing component; b) and c) Diagram of the device sensing mechanism with equivalent circuitry (R_c: contact resistance at electrode/conductive sphere interface and R_s: bulk resistance of conductive sphere); d) Mechanical-resistance response of the device to an external loading; e) Digital image of a typical flexible pressure sensing film with 4×4 detecting units and an 8×8 mm^2 spatial resolution.

2. Experimental

2.1 Material preparation

For the preparation of the pre-cured SWCNT/PDMS mixtures, first, carboxyl group (−COOH) functionalized SWCNT (out diameter = 1 - 4nm, inner diameter = 0.8-1.6 nm, length = 3-30 um, purity > 90 %, CheapTubes Inc.), a PDMS base (Sylgard 184, Dow Corning) and ethyl acetate (Sigma) were homogenized by sonication at 20 kHz, 500 W for 2 h. (at a ratio of 1 mL of ethyl acetate for each 1 g PDMS base). Second, the PDMS curing agent (1:40 ratio for curing agent to base) were added to above mixture, and blended with glass rod for 15 minutes. Then, air bubbles in the mixture was removed under mild vacuum for 20 minutes.

For the preparation of the conductive sphere, first, the as-prepared SWCNT/PDMS mixture was transferred to a plastic dish with a controlled thickness of 1 mm. Second, a superfine glass fiber with the diameter of 125 um was dipped into the mixture in the dish vertically, pulled out immediately, and placed uprightly at room temperature until the formation of sphere (about half an hour). Then, thermally cured at 90 ℃ for 3 h. Finally, the cured SWCNT/PDMS sphere with the diameter of 600 ± 20 μm can be obtained. (Fig.S1)

2.2 Device fabrication

For the preparation of the flexible sensing film, first, a 4×4 silver electrode array (electrodes are circular, diameter of each circular electrode = 6 mm, distance between every circular electrode = 8 mm) was patterned on PET film (thickness = 40 μm) by inkjet printing as bottom skin, as shown in Fig. S2. Meanwhile, a regular ITO-coated PET film (sheet resistance = 60 ohm/sq, PET thickness = 125 μm, ITO thickness = 130 nm, transmittance > 79% at 550 nm of wavelength) with the same size was used as up skin. Second, a 6-layer stack of double sided tape (single-layer thickness = 100 μm, diameter of the hole = 6 mm) was put on the bottom skin as bonding frame. Third, the synthesized conductive spheres were positioned at the center of the holes. Then, the up skin was used to cover on the sphere and bonded by the stacked tape. Normally, the thickness of 6-layer stacked tapes is 0.591 mm. The difference between the thickness of the stacked tape and the diameter of conductive sphere will generates a small preload to ensure the contact between the conductive sphere and the bottom/up electrode. Finally, every electrode (16 circular electrodes in the bottom skin and one electrode in the up skin) was connected with copper wires using silver paste. More details can be seen in Fig. 1a. A typical flexible pressure sensing film with 4×4

detecting units was shown in Fig.1e, as well as its equivalent circuit mode in Fig. S3.

2.3 Characterization and measurements

The synthesized SWCNT/PDMS elastomer composites were characterized by scanning electron microscopy (SEM, Quanta 600, FEI Company) for morphology analysis and 4-point probe system (Pro4-440N, Lucas Labs) for sheet resistance. For the mechanical-resistance response of the conductive sphere and the fabricated flexible sensing film, a home-made measuring system was used. This system infcludes a PC-controlled universal test machine (Instron 5944 with a 5 N load cell, ± 0.5 % of reading down to 1/250 to the load cell capacity) and a PC-recordable multimeter (Agilent 34401A). During this test, the central loading was used. The diameter of the force tips were 2.5 mm, 5.5 mm, and 8.5 mm, corresponding to the relevant diameter of the sensing area (3 mm, 6 mm, 9 mm), respectively. (Fig. S4) The efficiency of the flexible pressure sensing film was investigated by applying finger pressures at different locations, and further demonstrated through monitoring the fingertip pulse signals, jugular venous pulse (JVP) signals and wrist pulse signals of the testers of different ages.

3. Results and discussion

3.1 Theoretical consideration

Fig.1a illustrates the assembling structure of the flexible pressure sensing film. The working mechanism of this device with equivalent circuitry ($R_t = 2R_c + R_s$) was presented in Fig.1b, 1c, 1d. In this equivalent circuitry, conductive sphere was regarded as a resistive element (R_s), the contact resistance at conductive sphere/electrode interface was seen as (R_c), and total resistance (R_t). Specifically, when an external load is pressed against the bottom/up skins, the force-sensing electrode film experience shape deflection, and these sensitive spheres will deform accordingly. This leads to the change of contact area between conductive spheres and electrodes, and finally manifesting out by the variations of R_c and R_s. For this device itself, it is point contact between conductive sphere and electrode membrane without any pretreatment. This geometry determines the large variation of R_c under even a small external pressure. Meanwhile, the piezoresistive effect from conductive sphere, especially at the contact interface, further enhance this resistance response. In Fig.1b, this feature was further described by the current density variation before and after loading under the same voltage.

According to above description, the variations of contact area is directly determined by the deflection of electrode membrane. Based on the classic thin-plate theory, [23, 24, 25] small deflection (y_m) of the electrode membrane under an external loading (P) can be mathematically predicted, as seen in formula (1). This formula presents that the membrane physical properties (like thickness-t, Young's modulus-E, Poisson's ratio-v, and the diameter of sensing electrode-α) can play a considerable role in sensing performance of final device.

$$y_m = \frac{3a^4(1-v^2)}{16Et^3}P \quad \text{---------(1)}$$

In conclusion, the device sensitivity of mechanical-resistance response is mainly up to the physical properties of electrode membrane and conductive sphere. Formula (1) will provide an expected guidance for the performance optimization and geometry design of the device in the following experiments.

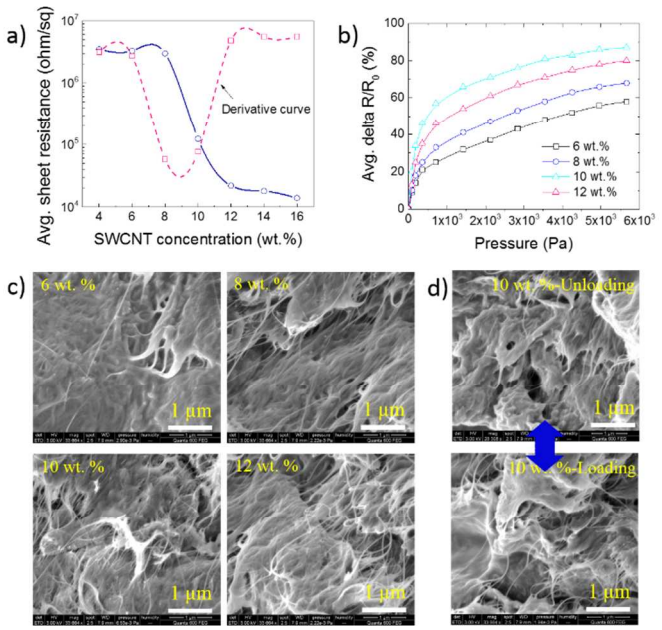

3.2 Material Preparation

Fig. 2 a) Sheet resistance of SWCNT/PDMS elastomers; b) Mechanical-resistance response of conductive SWCNT/PDMS sphere (Diameter = 600 ± 20 um); SEM images of c) SWCNT/PDMS elastomers with different SWCNT concentration, and d) The distribution of SWCNT in PDMS matrix before and after loading (10 wt. %).

As mentioned above, material sensitivity has an important effect on the optimal device performance. Herein, SWCNT was used to prepare PDMS based composite elastomer and the relevant conductive sphere. [26, 27] From Fig. 2a, when the concentration of SWCNT is between 8 -10 wt. %, the fastest change rate of sheet resistance can be observed from its derivative curve.

Mechanical-resistance response tests of conducive SWCNT/PDMS sphere were also investigated to optimize its dynamic piezoresistive sensitivity, as seen in Fig. 2b. It shows that the prepared conductive spheres with different SWCNT concentrations exhibited the large resistance variation under the external loading from 0 kPa to 5 kPa. Especially when the SWCNT concentration is 10 wt. %, the results demonstrated their ultrasensitive properties. Specifically, when the external

loading is 1 kPa, the resistance variation is up to 35 %. This value is about 1.7 times of that of conductive sphere (6 wt. %, SWCNT concentration), and 1.3 times of that of conductive sphere (12 wt. %, SWCNT concentration), respectively. Microscopic analysis was also used to analyse these results in Fig. 2c. It can be found that SWCNTs have a uniform dispersion in PDMS matrix, even single SWCNT can be distinguished. It indicated that the solvated preparation for SWCNT/PDMS elastomer composites is practical to obtain well physical mechanical performance and to fabricate the conductive percolation network. The results also shown that the amount of SWCNTs is increasing with its concentration increased from 6 wt. %, 8 wt. %, 10 wt. %, to 12 wt. %. Moreover, the concentration variation of SWCNT in PDMS matrix before and after loading is evident (Fig. 2d). This phenomenon demonstrated that the piezoresistive effect plays an important role in the resistance variation of the compressed conductive sphere, as well as in the sensitivity of the final device. Conclusively, conductive sphere with SWCNT concentration of 10 wt. % was used in the following test.

3.3 Characterization of the sensitivity

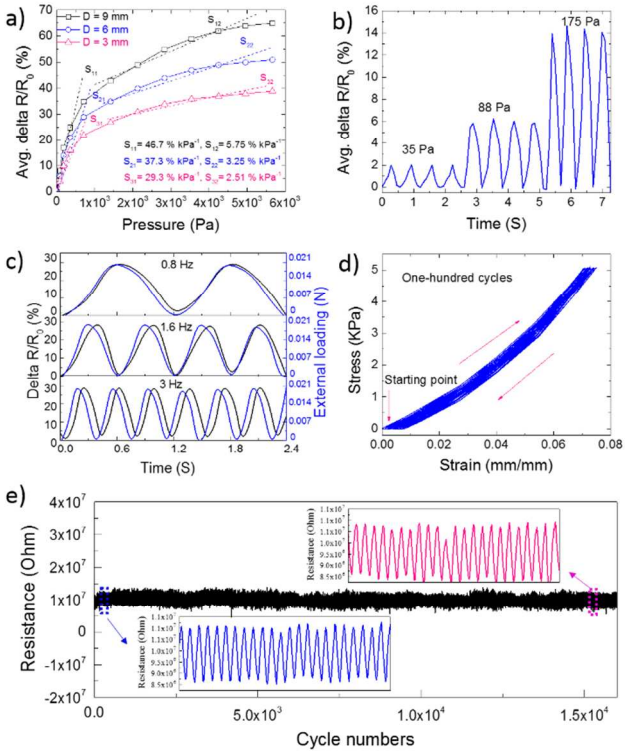

Fig. 3 Characterization of the mechanical-resistance response of the pressure sensor. a) Sensitivity with different sensing area (Diameter = 3 mm, 6 mm, 9 mm, respectively); b) Multi-cycle tests of dynamic loading/ unloading pressure with different values; c) Resistance response at different frequency of 0.8 Hz, 1.6 Hz, 3 Hz, separately; d) One-hundred consecutive compression test; e) Durability rest. The default diameter of sensor area = 6 mm, the diameter of conductive sphere = 600 ± 20 μm, the test rate = 1.6 Hz, the applied dynamic loading of 0.02 N with a preload = 0.01 N in all the tests if without special description.

As mentioned in theoretical consideration, device geometrical design is very crucial for the device sensing performance. Particularly, the thickness (t) of electrode film and the diameter (α) of the sensing area in every detecting unit, which are cubic function and quartic function to the final device sensitivity, respectively, as said by formula (1). Thus, a silver patterned PET film with the thickness of 40 um was used as bottom skin, which has great flexibility and can be well attached to the skin for subtle pressure perception. (Fig.S2) Meanwhile, an ITO coated PET film (thickness = 125 um) was used as up skin for support. In the following, a typical detecting unit in the flexible pressure sensing film was chose, and its sensitivity with different diameters of the sensing area was investigated systematically by the mechanical-resistance response.

In specific, the device sensitivity is evaluated as the resistance variation ($\Delta R/R_0 = (R_0-R_p)/R_0$, where R_0 and R_p is the resistance without and with applied pressure, respectively) over the external pressure loading (P) in Fig. 2a. Results show that the resistance variation is increasing with the increase of the external loading, whereas the device sensitivity is decreasing. Thus, the sensitive curves with two segments was observed. This phenomenon can be explained that the high external loading will generate the large deformation of sensing electrode membrane. At this time, the high shear force from the edge of the sensing membrane can't be ignored, leading to the deviation of the device sensitivity from linear relationship with the external loading. Moreover, when the diameter of the sensing area increases from 3 mm, 6 mm, to 9 mm, the sensitiviy of the device increases from 29.3 % kPa^{-1}/2.51 % kPa^{-1}, 37.3 % kPa^{-1}/3.25 % kPa^{-1}, to 46.7 % kPa^{-1}/5.75 % kPa^{-1}, respectively. This results can be clarified by formula (1). The deformation of circular membrane with edge clamped not only is up to the flexural rigidity of the membrane itself, but also is close relationship with the diameter of the circular membrane. So, the high diameter will bring large deformation of the sensing membrane under the same external loading, showing a high sensitivity.

3.4 Characterization of the cycle test

As for a pressure sensor, its working durability, detection accuracy and response frequency to an external loading are very significant. The relevant results were summarized in Fig. 3b, 3c, 3d and 3e. Fig. 3b shows the multi-cycle tests of dynamic loading/unloading pressure with different values to the sensors. Results exhibit that every response profile with different loading cycles (35 Pa, 88 Pa, 175 Pa, respectively) is very regular, stable and continuous. Response frequency of the prepared sensors to external loading was demonstrated in Fig. 3c. The output resistance signals were compared with the dynamic force inputs at different frequencies. It can be observed that the resistance response signals remained very stable without evident change. Even when the frequency is up

to 3 Hz, it still can be coincident with the input force waves well. This phenomenon indicated that the SWCNT/PDMS elastomer exhibits excellent physical viscoelasticity. Great working durability of our pressure sensing unit was presented in Fig. 3e. From the whole cyclic curve, the high signal-to-noise ratios were well maintained. The cyclic profiles at the beginning and those after fifteen-thousand times of loading–unloading cycle were compared. From the results, the resistance amplitude exhibited the negligible changes.

The mechanical properties of this device was also assessed, arming to explaining the above great performance. [28, 29] We measured the compressive stress (σ, the applied force divided by the overlapping area) as a function of strain (ε, the compressed distance divided by the diameter of the conductive sphere). The plotted curves (σ versus ε) for a typical one-hundred loading/unloading cycles of the device were exhibited in Fig. 3d. The almost overlapping cyclic curve was presented. The maximum σ and ε values in the loading cycles were 5 kPa and 7 %, separately. An effective elastic modulus (E) can be calculated by the slope of the stress versus strain plot, which is strongly influenced by the concentration and morphology of SWCNT in PDMS matrix, the geometry structure of the elastomer, and the ration of curing agent/PDMS base. It can be obtained this elastomer sphere showed a very low E at a low pressure of 1.5 kPa, about 0.07 MPa, compared with typical value 0.36 MPa of PDMS. This data is also lower than many of the values reported, such as the modulus of polymer based foam and hydrogel. [28, 30] Therefore, the optimized elastomer sphere with low modulus and great viscoelasticity contributes to the excellent compressive cyclic performance of the device. It can be concluded that the developed flexible pressure sensing film can be used to detecting pressure signals continuously, showing high accuracy and satisfied response capability.

3.5 Surface Topology Sensing

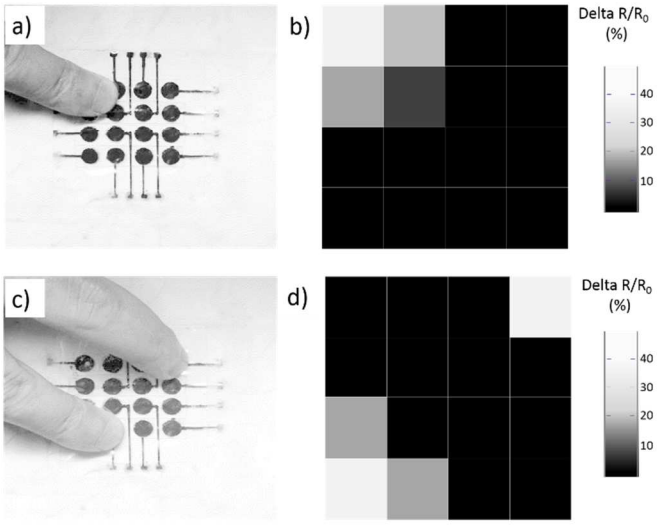

Fig. 4 a) and c) Digital image of the fingers on the surface of the pressure sensing film to test the figure pressure-sensing capability; b) and d) Finger pressure distribution presented by resistance variation of every detecting unit.

To verify the efficiency of this device, the flexible pressure sensing film by 4×4 detecting units with an 8×8 mm^2 spatial resolution was used to mapping the finger pressure, as shown in Fig. 4a and 4c. The equivalent circuit pattern of this flexible pressure sensing film was presented in Fig. S3, in which every detecting unit can be regards as a chip-type sensing component. The detected pressure signals were recorded and plotted as a colour intensity map (Fig.4b and 4d). Each square represents the relevant detecting unit. The colour intensity corresponds to the resistance variation of this detecting unit under the external loading. Results show that this device can detect the amplitudes and distributions of multiple finger pressures accurately at the same time. It also can convey the locations of the fingers on this device precisely. This capability is the typical feature of electronic skin. [31] In addition, the resolution of the present pressure sensing film is centimeter-scale, which also can be reduced to millimeter-scale or micro-scale via an advanced photo-lithography technique according to the requirements.

3.6 Monitoring of human pulse signals

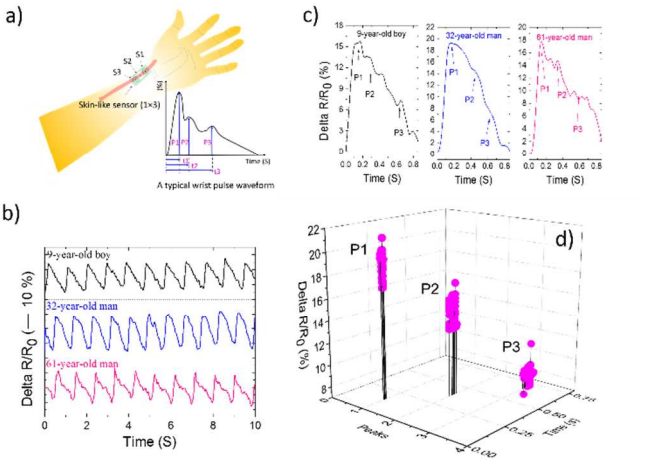

Fig.5 a) A detailed schematic showing how the wrist pulse was monitored using flexible pressure sensing film (1×3); The inset illustration shows the typical waveform of wrist pulse; b) and c) Real-time resistance-response measurement with different aged testers (9-year-old boy, 32-year-old man, and 61-year-old man, respectively); d) Statistical distribution of key data (P_1, P_2 and P_3 with the relevant time intervals) from the tester of 61-year-old man.

To further verify the functionality of the prepared pressure sensing film here, fingertip pulse singles, jugular venous pulse (JVP) signals and wrist pulse signals were continuously tracked. The measuring results of fingertip pulse signals and JVP signals can be seen in Fig. S5 and S6. [13, 32] Fig.5a presented a detailed illustration of how the monitoring of pulse signals at wrist was performed. The optimal tracked position was evaluated by this device (1×3, S_1, S_2, and S_3) to find the

strongest resistance response. Moreover, a typical wrist pulse waveform was shown in the inset illustration of Fig.5a, which is mainly consisted of three characteristic peaks. These peaks are known as being closely related with the heart activities. [33, 34]

Fig.5b presents the continuous pulse recordings from three different testers. Results shown that the maximal resistance variation was around 16.8 for 9-year-old boy, 22.2 for 32-year-old man, 20.1 for 61-year-old man, respectively. The corresponding heart rate is about 65 cycles/minute, 66 cycles/minute, 63 cycles/minute, separately. This was the basic difference information we can obtain from the pulse recordings. A close-up analysis of a single cardiac cycle with these different testers was provided in Fig. 5c. Every cycle waveform has been characterized into three peaks (P_1, P_2, and P_3). Clinically significant parameters, such as the radial augmentation index (P_2/P_1) and the reflection index (P_3/P_1), can be directly extracted and computed from these pulse recordings. [35] In addition, a continuous pulse recordings for one minute from the tester of 61-year-old man were investigated. The key data (P_1, P_2, and P_3 with the relevant time intervals) was taken out, and was further plotted into a 3-diametrational image (Fig.5d). Generally, accurate detection and collection of this data will be very promising for the establishment of a complete system used for heart disease analysis.

4. Conclusions

In summary, a new kind of flexible pressure sensing film was designed and fabricated based on conductive SWCNT/ PDMS sphere successfully. These conductive spheres were prepared by dipping method, and were further sandwiched by flexible electrodes using a stacked double-sided tape. The sensitive mechanism was mainly based on the contact resistance of conductive sphere/electrodes interface and the piezoresistive effect of conductive sphere. The developed sensing film displayed a maximum sensitivity of 46.7 % kPa^{-1}, durability over 15,000 cycles, and very rapid mechanical responses (a few milliseconds) with the defined parameters. Our sensing film demonstrated its capability to detect and convey the location and distribution of one or more external loadings at the same time accurately. We also demonstrate that the developed flexible pressure sensing film can be used to monitoring real-time fingertip pulse signals, human jugular venous pulse (JVP) signals and wrist pulse signals for different aged testers. These great performance highlights their potential application not only for patients as disease diagnosis, but also for health people as the diet and exercise guidance in daily life.

Acknowledgements

We express gratitude to the key discipline fund of Shanghai (B117).

Notes and references

Department of Materials Science, Fudan University, Shanghai 200433, China. *Corresponding author E-mail: zgyang@fudan.edu.cn

1. X. Wang, H. Zhang, R. Yu, L. Dong, D. Peng, A. Zhang, Y, Zhang, H, Liu, C, Pan, and Z. L. Wang, Adv. Mater., 2015, DOI: 10.1002/adma.201405826.
2. E. Lumpkin, and M. Caterina, Nature, 2007, 445, 858.
3. K. Takei, T. Takahashi, J. C. Ho, H. Ko, A. G. Gillies, P. W. Leu, R. S. Fearing, and A. Javey, Nat. Mater., 2010, 9, 821.
4. T. Sekitani, T. Yokata, U. Zschieschang, H. Klauk, S. Bauer, K. Takeuchi, M. Takamiya, T. Sakurai, and T. Someya, Science, 2009, 326, 1516.
5. M. Segev-Bar, G. Konvalina, and H. Haick, Adv. Mater., 2015, 27, 1779.
6. J. Jeong, M. Kim, H. Cheng, W. Yeo, X. Huang, Y. Liu, Y. Zhang, Y. Huang, and J. Rogers, Adv. Healthc. Mater., 2014, 3, 621.
7. S. Gong, W. Schwalb, Y. W. Wang, Y. Chen, Y. Tang, J. Si, B. Shirinzadeh, and W. L. Chen, Nat. Commun. 2014, 5, 3132.
8. C. Wang, D. Hwang, Z. Yu, K. Takei, J. Park, T. Chen, B. Ma and A. Javey, Nat. Mater., 2013, 12, 899.
9. D. J. Lipomi, M. Vosgueritchian, B. C. K. Tee, S. L. Hellstrom, J. A. Lee, C. H. Fox and Z. Bao, Nat. Nanotechnol., 2011, 6, 788.
10. X. Wang, Y. Gu, Z. Xiong, Z. Cui, and T. Zhang, Adv. Mater., 2014, 26, 1336.
11. T. Someya, Y. Kato, T. Sekitani, S. Iba, Y. Noguchi, Y. Murase, H. Kawaguchi, and T. Sakurai. Proc. Natl Acad. Sci., 2005, 102, 12321.
12. K. Adil, H. Anne, M. Guillaume, and A. Pierre, J. Biomed. Opt., 2015, 20, 051010.
13. C. Pang , J. Koo , A. Nguyen, J. M. Caves, M. Kim, A. Chortos, K. Kim, P.J. Wang, J. Tok, and Z. Bao, Adv. Mater., 2015, 27, 634.
14. L. Li, S. Mac-Mary, D, Marsaut, J.M. Sainthillier, S. Nouveau, T. Gharbi, O. de Lacharriere, and P. Humbert, Arch. Dermatol. Res., 2006, 297, 412.
15. Y. L. Tai, and Z. G. Yang. J. Mater. Chem., 2011, 21, 5938
16. Y. Zang, F. Zhang, D. Xi, K. Gao, C. Di, and D. Zhu, Nat. Commun., 2015, 6, 6269.
17. J. Park, Y. Lee, J. Hong, M. Ha, Y. Jung, H. Lim, S. Kim, and H. Ko, ACS nano, 2014, 8, 4689.
18. S. C. B. Mannsfeld, B. Tee, R. M. Stoltenberg, C. V. Chen, S. Barman, B. V. O. Muir, A. N. Sokolov, C. Reese, and Z. Bao, Nat. Mater., 2010, 9, 859.
19. J. Wang, J. Jiu, M. Nogi, T. Sugahara, S. Nagao, H. Koga, P. He, and K. Suganuma, Nanoscale, 2015, 7, 2926.
20. T. Ioppolo, and M. V. Ötügen, Opt. Lett., 2010, 35, 2037.
21. Y. Tanaka, K. Sato, T. Shimizu, M. Yamato, T. Okano, and T. Kitamori, Lab Chip, 2007, 7, 207.
22. T. Ioppolo, U. K. Ayaz, M. V. Ötügen, J. Appl. Phys., 2009, 105, 013535.
23. B. Nie, R. Li, J. Brandt, and T. Pan, Lab Chip, 2014, 14, 1107.
24. R. W. Ellis, and C. W. Smith., Exp. Mech., 1967, 7, 372.
25. D. W. Zietlow, D. C. Griffin, and T. R. Moore, AIP Adv., 2012, 2, 042103.
26. H. Lee, J. K. Yoo, J. H. Park, J. H. Kim, K. Kang, and Y. S. Jung, Adv. Energy Mater., 2012, 2, 976.
27. J. Lee, K.Y. Lee, M. Gupta, T. Kim, D. Lee, J. Oh, C. Ryu, W. Yoo, C. Kang, S. Yoon, J. Yoo, and S. Kim, Adv. Mater., 2014, 26, 765.
28. L. Pan, A. Chortos, G. Yu, Y. Wang, S. Isaacson, R. Allen, Y. Shi, R. Dauskardt, and Z. Bao, Nat. Commun., 2014, 5, 3002.

29. K. Nawaz, U. Khan, N. Ul-Haq, P. May, A. O'Neill, and J. N. Coleman, Carbon, 2012, 50, 4489.
30. H. Yao, J. Ge, C. Wang, X. Wang, W. Hu , Z. Zheng, Y. Ni, and S. Yu, Adv. Mater., 2013, 25, 6692.
31. S. Harada, K. Kanao, Y. Yamamoto, T. Arie, S. Akita, and K. Takei, ACS Nano, 2014, 8, 12851
32. T. Nguyen, A. Dinh, F.M. Bui, and T. Vo., IFMBE Proceedings, 2015, 26, 75
33. Y. Yim. Journal of Korean Medicine, 2014, 35, 19
34. G. Schwartz, B. Tee, J. Mei, A.L. Appleton, D. Kim, H. Wang, and Z. Bao, Nat. Comm., 2012, 4, 1859.
35. M. Elgendi. Current Cardiology Reviews, 2012, 8, 14.

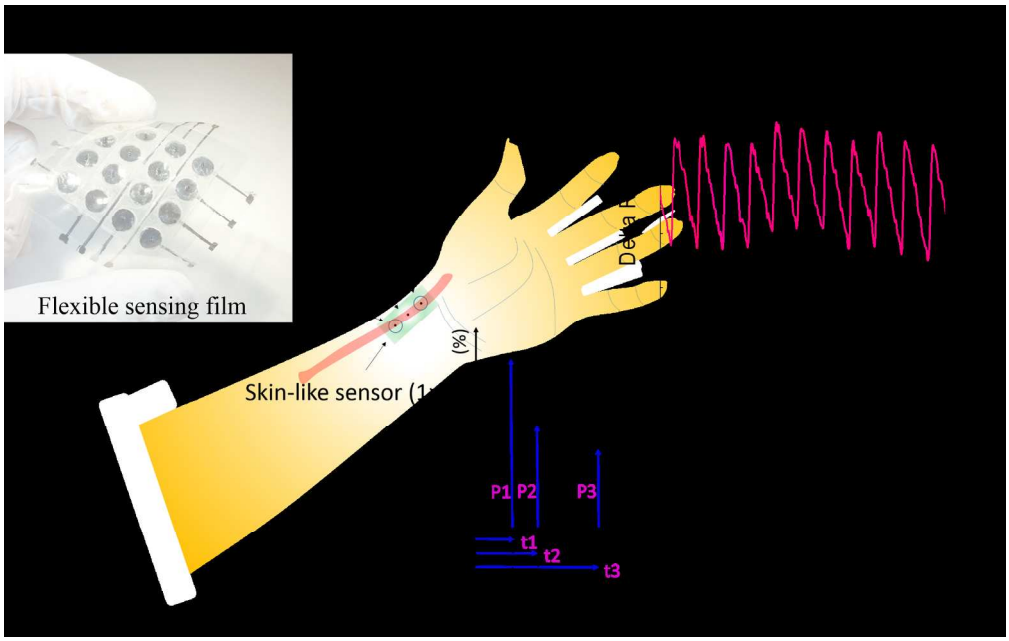

399x252mm (150 x 150 DPI)